Physics Letters B 702 (2011) 121–126

Contents lists available at ScienceDirect

Physics Letters B

www.elsevier.com/locate/physletb

Two-body photodisintegration of ^{3}He between 7 and 16 MeV

W. Tornow [a,b,*], H.J. Karwowski [c,b], J.H. Kelley [d,b], R. Raut [a,b], G. Rusev [a,b], S.C. Stave [a,b,1], A.P. Tonchev [a,b], A. Deltuva [e], A.C. Fonseca [e], L.E. Marcucci [f,g], M. Viviani [g], A. Kievsky [g], J. Golak [h], R. Skibiński [h], H. Witała [h], R. Schiavilla [i,j]

[a] Duke University, Durham, NC 27708-0308, USA
[b] Triangle Universities Nuclear Laboratory, Durham, NC 27708-0308, USA
[c] University of North Carolina at Chapel Hill, Chapel Hill, NC 27599-3255, USA
[d] North Carolina State University, Raleigh, NC 27695-8202, USA
[e] Centro de Fisica Nuclear da Universidade de Lisboa, P-1649-003 Lisboa, Portugal
[f] Department of Physics, "Enrico Fermi", University of Pisa, I-56127 Pisa, Italy
[g] INFN, Sezione di Pisa, I-56100 Pisa, Italy
[h] M. Smoluchowski Institute of Physics, Jagiellonian University, PL-30059 Kraków, Poland
[i] Department of Physics, Old Dominion University, Norfolk, VA 23529, USA
[j] Thomas Jefferson National Accelerator Facility, Newport News, VA 23606, USA

ARTICLE INFO

Article history:
Received 3 May 2011
Received in revised form 27 May 2011
Accepted 27 June 2011
Available online 8 July 2011
Editor: D.F. Geesaman

Keywords:
Electromagnetic reaction
Giant dipole resonance of light nuclei
Two-body breakup cross section
Meson-exchange currents
Three-nucleon forces
Coulomb interaction

ABSTRACT

A comprehensive data set is reported for the two-body photodisintegration cross section of ^{3}He using mono-energetic photon beams at eleven energies between 7.0 and 16.0 MeV. A ^{3}He + Xe high-pressure gas scintillator served as target and detector. Although our data are in much better agreement with our state-of-the-art theoretical calculations than the majority of the previous data, these calculations underpredict the new data by about 10%. This disagreement suggests an incomplete understanding of the dynamics of the three-nucleon system and its response to electromagnetic probes.

The three-nucleon (3N) system provides a unique laboratory for testing our understanding of the nuclear Hamiltonian. In particular, the study of electromagnetic processes gives information on nuclear currents, which cannot be obtained from investigating pure hadronic processes. The nuclear currents are closely related to the underlying nuclear forces via the continuity equation. While pairwise nucleon–nucleon (NN) interactions invoke two-body meson-exchange currents, 3N force (3NF) terms in the nuclear Hamiltonian lead to three-body contributions to the nuclear current. As a result, nuclear reactions initiated with photons as a probe provide the most complete test of theoretical models of NN and 3N forces and their associated currents.

Although computational techniques for 3N systems studied with electromagnetic probes are highly developed, a consistent treatment of nuclear interactions and nuclear currents still presents a challenge. Only very recently, Chiral Effective Field Theory has provided the theoretical framework needed to treat electromagnetic nuclear processes in a consistent way [1,2]. Currently, theoretical work is in progress to implement this new scheme. Therefore, accurate experimental data for electromagnetic 3N reactions, especially the ^{3}He$(\gamma, p)^2$H reaction, are of considerable interest to guide this new theoretical approach.

The first ^{3}He$(\gamma, p)^2$H cross-section measurements have been reported more than half a century ago. Although experimental techniques have improved since the very early studies, the data obtained later during the 60s and 70s using a variety of experimental approaches disagree widely with each other. As a result, the modern theoretical approaches, which all agree within less than 10%, are in disagreement with the majority of the existing experimental cross-section data.

* Corresponding author at: Duke University, Durham, NC 27708-0308, USA.
E-mail address: tornow@tunl.duke.edu (W. Tornow).
[1] Present address: Pacific Northwest National Laboratory, Richland, WA, United States.

0370-2693
doi:10.1016/j.physletb.2011.06.080

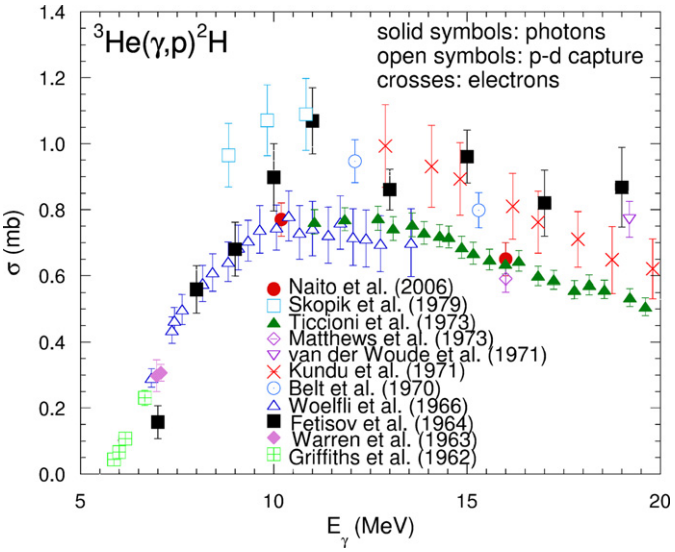

Fig. 1. (Color online.) Existing data for the total cross section of the reaction ^{3}He$(\gamma, p)^2$H. Solid dot [4], open upside triangle [5], solid diamond [6], solid square [7], open square [8], open diamond with horizontal line [9], open inverted triangle [10], open dot with center point [11], cross [12], solid upside triangle [13], open square with center cross [14].

Fig. 1 summarizes the status of the cross-section data for the ^{3}He$(\gamma, p)^2$H reaction. It covers a time span of almost half a century, although only two data points were reported after the year 1979. The available experimental data sets are in good agreement with each other up to an incident γ-ray energy of about 8.5 MeV. However, above this energy, they split into two distinct bands, which are inconsistent with each other, and provide average cross-section values which differ by about 25%. In the following we focus on this energy regime. Four different data sets form the lower band, while five different data sets contribute to the upper band. Clearly, considering the uncertainties associated with the data, the lower band appears to represent the true ^{3}He$(\gamma, p)^2$H cross section.

The data shown in Fig. 1 by solid symbols were obtained with incident photons, while the data given by open symbols were derived from radiative capture experiments (the time-reversed reaction) using the principle of detailed balance. Finally, the crosses show a data set based on the electro-disintegration of ^{3}He, but converted to photodisintegration cross-section values. Common to all absolute cross-section measurements is the challenge of determining the number of incident projectile particles, the number of target nuclei, and the number of ejectile particles. However, the techniques used to measure these quantities and to determine their uncertainty differ considerably for the results shown in Fig. 1.

The data with real photons as projectiles can be grouped into two classes. Here, the majority of the data were taken with bremsstrahlung beams (Warren et al., Fetisov et al., and Ticcioni et al.), while the recent two data points of Naito et al. at 10.2 and 16 MeV were obtained with a mono-energetic photon beam. The data of Fetisov et al. (solid squares), which are part of the upper band, have fairly large overall uncertainties (∼20%), while the data of Ticcioni et al. (solid upside triangles) and Naito et al. (solid dots), which are the main contributors to the lower band, have much smaller overall uncertainties (∼7% in both cases) and nicely agree with each other. The bremsstrahlung beam of Ticcioni et al. was produced by passing high-energy electrons through a gold radiator foil. The photon intensity was calculated from the measured electron beam charge using the Bethe–Heitler formula. The mono-energetic photons of Naito et al. were generated via Compton backscattering of an external laser from electrons stored in a storage ring. While a magnetic spectrometer with focal plane detectors was used for detecting deuterons in the experiment of Ticcioni et al., Naito et al. used a time-projection chamber to record both the protons and deuterons from the breakup of ^{3}He, *i.e.*, the target and detector were identical. The incident photon flux was measured with a NaI detector operated in a special pile-up mode. Naito's group used the same method and setup to measure the two-body breakup cross section of ^{4}He and they obtained "unphysically" low cross-section values below 27 MeV [3], which may cast some doubt on the reliability of the otherwise very beautiful approach of Naito et al. It may also be of interest to point out that the cross-section values of Ticcioni et al. are the result of a difference measurement of the deuteron yields recorded with the radiator both in and removed from the electron beam.

The radiative capture experiments can also be grouped into two categories. One, in which the high-energy γ rays from the $d+p$ or $p+d$ capture reactions are detected with large NaI detectors, and the other one in which the associated ^{3}He ions are recorded using a magnetic spectrometer equipped with focal plane detectors. The former approach was used by Wölfli et al. (open upside triangles) and Skopik et al. (open squares). The quoted overall uncertainty is about 10% in both cases in the energy region of overlap, while the uncertainty of the data of Wölfli et al. increases to 15% at their highest energy. In this type of experiment the challenge lies in the determination of the γ-ray detection efficiency. Clearly, the data of Wölfli et al. and Skopik et al. are in disagreement with each other. The approach pioneered by Belt et al. avoids the detection of γ rays and instead relies on the detection of the associated ^{3}He ions in a magnetic spectrometer with position sensitive detectors mounted in the focal plane. Therefore, the charged-particle detection process is identical to that used for incident photons by Ticcioni et al. The two data points of Belt et al. (open circles) are shown in Fig. 1 near 12 and 15 MeV. Their overall uncertainty is about 7%. These data clearly belong to the upper band and are inconsistent with those of Ticcioni et al. Belt's group used its method also at higher energies, resulting in the datum of van der Woude et al. (upside down open triangle) near 19 MeV, which also belongs to the upper band. Subsequently, the method of Belt et al. was used by Matthews et al. However, their result near 16 MeV (open diamond) belongs to the lower band and has an overall uncertainty of about 6%, the smallest quoted uncertainty of all available data. Surprisingly, this very attractive approach, which involves only charged particles, appears to have its own problems, otherwise the data of Belt et al. and Matthews et al. in the 15 to 16 MeV energy range should agree better. The main difference between the two data sets is the fact that the former uses the reaction ^{1}H$(d, ^3$He$)\gamma$, while the latter uses the reaction ^{2}H$(p, ^3$He$)\gamma$ which results in less background in the ^{3}He spectra.

Finally, the electro-disintegration data of Kundu et al. are shown as crosses in Fig. 1. They have an estimated uncertainty of about 15% and belong to the upper band. The protons and deuterons from the breakup of ^{3}He were detected with a magnetic spectrometer and solid state detectors in its focal plane. The long wavelength approximation was used to convert the measured electro-disintegration cross section into the photodisintegration cross section.

Based on the information given in the literature and discussions with leaders in the field, who are responsible for some of the data shown in Fig. 1, it is virtually impossible even for the most experienced researcher in the electromagnetic nuclear physics community to determine what could have gone wrong in some of the experiments described above. Clearly, statistics is not the issue. One must conclude that unaccounted for systematic effects have prevented experimentalists from providing their theory colleagues

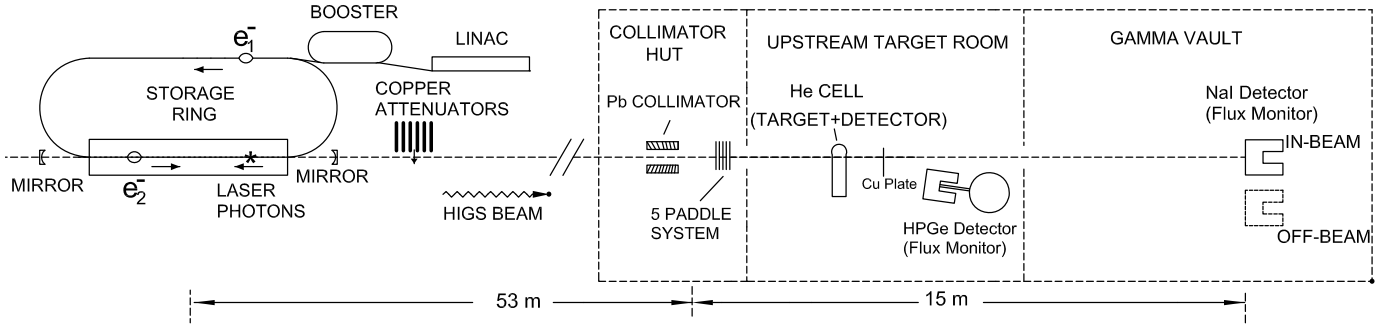

Fig. 2. Diagram of the HIγS facility layout.

with an accurate and experimentally determined cross section to which they can compare their calculations for this important few-body reaction.

In view of Fig. 1, one may question whether any additional new measurements will clarify the experimental situation, *i.e.*, whether the few-body physics community will ever settle on a definite and accurate experimentally determined value for the ^{3}He$(\gamma, p)^2$H cross section. However, despite this uncertainty, experimental few-body physics should not stop from finding the true cross section. Clearly, some of the data shown in Fig. 1 are incorrect and should be ignored. A fresh look at the ^{3}He$(\gamma, p)^2$H reaction by a group of experimentalists, who have experience in state-of-the-art photon production as well as photon and charged-particle detection techniques may result in an important step aimed at narrowing the present scatter in the cross-section data. Such an unbiased approach by a group that has no stake in any of the previous data may help to eliminate some of the existing data, thus hopefully providing theory with a considerably reduced band of so-called recommended experimental data. This is the aim of the present work. With a different experimental technique at hand, a new approach was undertaken, and the resulting data for the ^{3}He$(\gamma, p)^2$H cross section are reported in this Letter. They are compared to the most recent calculations which are based on different and independent theoretical approaches.

Mono-energetic photons were produced at the upgraded High-Intensity γ-ray Source (HIγS) (see Fig. 2) of the Duke University Free Electron Laser Laboratory (DFELL), which is operated by the Triangle Universities Nuclear Laboratory (TUNL). Data were obtained in two runs: the first run took place in June of 2008 at 8.8, 9.9, 10.9, 11.8 and 12.8 MeV, while the second run took place in May of 2010 at 7.0, 7.9, 12.0, 14.0, 15.0, and 16.0 MeV. In addition a short test run was performed in December 2010 to cross-check some of our results. The photon beams were generated via Compton backscattering of FEL photons from relativistic electrons in one of the two straight sections of the DFELL electron storage ring. The electron energy was changed between 424 MeV and 644 MeV and the wavelength of the FEL photons produced by the OK-5 undulator was varied between 453 nm and 463 nm to generate the photon energies of interest. Using the booster injector, the electron beam current in the storage ring was kept constant at either 60 mA or 70 mA. In addition, the FEL power was kept constant to guarantee a constant photon flux at each individual photon energy. The energy spread ΔE_γ (FWHM) of the photon beams varied between 175 and 450 keV at $E_\gamma = 7.0$ and 16.0 MeV, respectively.

The target and detector system consisted of a high-pressure ^{3}He + Xe gas scintillator (see Fig. 3) to detect the protons and deuterons from the two-body breakup reaction of ^{3}He($Q = -5.49$ MeV). A pure ^{3}He gas scintillator has only moderate energy resolution and, in addition, suffers from wall effects due to its low stopping power for protons and deuterons at the ^{3}He pressures

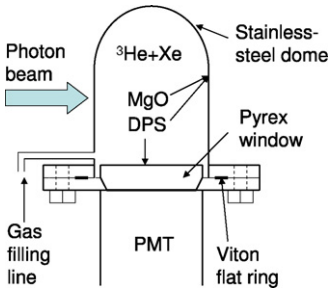

Fig. 3. Diagram of the ^{3}He + Xe gas scintillator cell.

available for the present experiments. For a given total pressure the xenon admixture can be optimized to provide the stopping power needed to minimize wall effects, and at the same time to yield sufficient pulse-height separation between pulses produced by the protons and deuterons of interest and those generated by electrons through Compton scattering of the intense incident photon flux in the detector gas and its stainless steel container of 1 mm wall thickness. The protons and deuterons are emitted preferentially into the angular range of 50° to 130° relative to the incident photon-beam momentum. For a total pressure of about 50 atm, a 4 : 1 ratio of ^{3}He to Xe gas is optimal for 10 to 13 MeV photons, while a 2 : 1 ratio is more suitable for energies above 13 MeV. A xenon partial pressure of 5 atm is the optimum pressure for photon energies of 9 MeV and below. Fig. 4 shows typical pulse-height spectra obtained with 10, 12.5 and 15 MeV photon beams using a 34 atm ^{3}He + 10 atm Xe gas scintillator. The peak to the right seen in the pulse-height distributions is due to protons and deuterons from the two-body breakup of ^{3}He. At 12.5 and 15 MeV this peak is well separated from the three-body breakup events of ^{3}He($Q = -7.69$ MeV). The large number of events observed at very low pulse heights is due to electrons produced by Compton scattering of the incident photons. At all energies there is a practically background-free region between the two-body and three-body breakup events. Information on ^{3}He + Xe gas scintillators can be found in Ref. [15]. Here, we only point out that in noble gas scintillators a well-defined portion of the charged-particle energy is converted into light. Therefore, in principle, the detection efficiency for charged particles is 100%. Only if a charged particle is created very close to the inside wall of the gas scintillator housing, may it run into the wall. As a result, it may not deposit all of its energy in the gas volume, thus leading to a smaller pulse height, which may not be in the region of interest. However, the associated losses of events due wall effects are very small in our case, and can easily be calculated (see below). It should also be noted that in contrast to plastic and liquid scintillators, the pulse height produced in gas scintillators by strongly ionizing particles depends only on the energy deposited in the gas and not on the type of

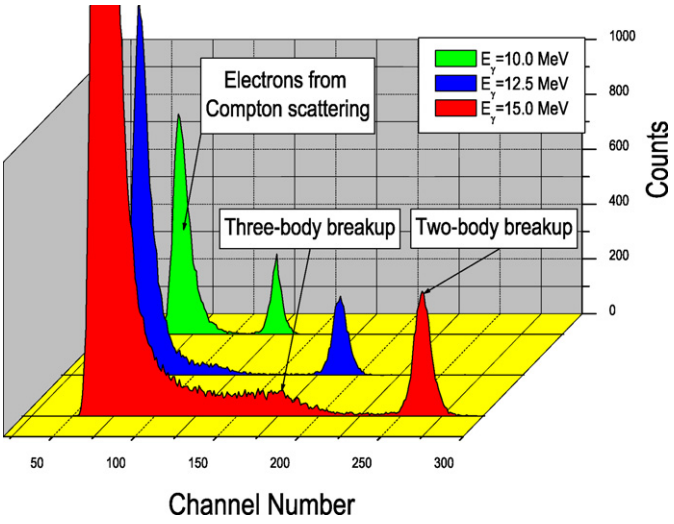

Fig. 4. (Color online.) Pulse-height distributions obtained with a 34 atm ^{3}He + 10 atm Xe gas scintillator for incident photon energies of $E_\gamma = 10.0$ MeV (back), 12.5 MeV (center) and 15.0 MeV (front). See text for details.

particle. For example, 5 MeV protons, deuterons, ^{3}He recoils, and α particles all give the same pulse height, if completely stopped in the gas volume. The energy resolution of high-pressure gas scintillators can be considerably better than that of plastic and liquid scintillators, provided special care is taken with respect to reflector material, wavelength shifters and purity of the gases used, among other more subtle details.

In order to correct our ^{3}He breakup data for photon-induced charged-particle reactions on xenon and the wall materials, we used an identical gas scintillator with the ^{3}He gas replaced by ^{4}He (with a breakup threshold of 19.81 MeV). The data taken with the ^{4}He + Xe gas scintillator showed that the background in the pulse-height region of interest due to photon-induced charged-particle reactions in the Xe gas, the thin MgO reflector and associated wavelength shifter deposited on the inner wall of the gas scintillator housing is less than 2% of the ^{3}He(γ, pd) yield at all energies investigated.

The incident photon flux measurement was accomplished with a NaI detector using the standard HIγS approach [16]. Briefly, because of the high photon flux (for example 1.3×10^7 γ/s at $E_\gamma = 12$ MeV) through the 1 cm diameter lead collimator, the NaI detector cannot be placed directly into the photon beam. Therefore, we calibrated the HIγS scintillator-paddle system located right after the collimator in the collimator hut (see Fig. 2). For this purpose three well-characterized copper blocks were inserted in the photon beam, each reducing the photon flux by a factor of about 10. They were positioned about 30 m upstream of our ^{3}He + Xe gas scintillator and inside of the shielding wall of the electron storage ring. With three attenuators inserted, the photon flux in the Gamma Vault (see Fig. 2) was low enough to place a standard 10″ diameter and 12″ long NaI detector directly into the beam at 0° to cross-calibrate the detector-paddle system. Due to its purposely low efficiency, under these conditions the detector-paddle system's count rate was 1 to 2 Hz (depending on photon energy). From the yield measured with the NaI detector at 0° and its known efficiency, the detector-paddle rate/photon conversion factors were determined for all our energies. Of course, corrections due to photon flux attenuation in air were applied, ranging for the 2010 measurements from 4.6% at 7.0 MeV to 3.5% at 16.0 MeV. As a side remark we mention that at this time we also placed a standard 123% High-Purity Germanium (HPGe) detector into the direct beam at 0° in order to determine the incident photon energy. For photon energies of 13 MeV and above the photopeak in the HPGe detector was not sufficiently separated anymore from the Compton continuum to provide an accurate photon energy determination. Therefore, we used the NaI detector at higher energies. It should be noted that the measured photon energies always agreed within 40 keV with the ones calculated from the electron storage ring and undulator parameters. While in the June 2008 cross-section measurements the gas scintillators were mounted in the Gamma Vault, for the 2010 runs they were positioned in the newly constructed Upper Target Room, which is located in front of the Gamma Vault (see Fig. 2).

Due to the upright cylindrical shape of our gas scintillator housing (see Fig. 3) with inner diameter of 5.5 cm, the determination of the effective target thickness requires the knowledge of the horizontal position of the photon beam, which is formed by the 1.0 cm diameter and 30.5 cm long lead collimator located about 4 m upstream of the gas scintillator in the well-shielded collimator hut. We determined the position and spatial dimensions of the photon beam at the location of the gas scintillator to 0.5 mm accuracy using the γ-ray imager and associated procedure described in Ref. [17].

From gates set around the proton and deuteron pulse-height distributions obtained at our incident photon energies, raw yields for the ^{3}He$(\gamma, p)^2$H reaction were obtained with statistical uncertainties of 1% or smaller. For $E_\gamma \geqslant 14.0$ MeV we inserted one of the copper attenuators to keep dead time and pile-up effects small. The yields were corrected for dead time (<2%), photon absorption in the gas scintillator front wall (~2.5% effect) and loss of pulses due to wall effects caused by the finite range of the protons and deuterons from the reaction of interest. Wall effects were included in our Monte Carlo simulation of the experimental setup by using calculated differential cross-section data for the ^{3}He$(\gamma, p)^2$H reaction for the energies of interest. The associated corrections were smaller than 0.2% at 6.98 MeV, and increased to about 1.6% at the higher energies. In our June 2008 run we accumulated data at $E_\gamma = 12.8$ MeV with both our standard 40.8 atm ^{3}He + 10.2 atm Xe gas scintillator as well as with the 30.6 atm ^{3}He + 20.4 atm Xe gas scintillator used in May 2010 at energies $\geqslant$13.0 MeV. The cross-section values obtained from these two measurements agreed within 1.3%. This is a very satisfactory result considering the statistical uncertainties of 0.8% in both measurements, estimated background subtraction uncertainties of 1.0% and 1.5%, respectively, and the fact that we cannot determine the exact amount of gas in our gas scintillators to better than 1%.

Incorrect cross-section values can be obtained by using an incorrect efficiency for the NaI detector employed in the photon flux determination. However, NaI detectors can be modeled with high precision using standard codes, and their accuracy has been experimentally confirmed. At γ-ray energies $\leqslant$10 MeV we also used our HPGe detector of known efficiency, but now positioned off-axis, and recorded during the actual ^{3}He$(\gamma, p)^2$H cross-section measurements the photons scattered into the HPGe detector from a thin copper plate placed in the 0° beam (see Fig. 2). The γ-ray flux determination derived from this method was consistent with our standard NaI-scintillator paddle approach within the estimated 6% uncertainty of the HPGe detector method. At γ-ray energies above 10 MeV, we used in addition to our standard approach, ^{197}Au foils placed at the exit of the lead collimator during the actual cross-section measurements. Again, within the associated uncertainties of less than 10%, the photon flux deduced from the ^{197}Au$(\gamma, n)^{196}$Au activation-foil measurements agreed with the one obtained with our standard approach.

Using the calculated efficiency of the NaI detector (~98%, exact value depending on photon energy and threshold) at the photon energies of interest, the cross-section values given in Table 1 and

Table 1
Results for the cross section of the ^{3}He(γ, p)^{2}H reaction.

E_γ (MeV)[a]	σ (mb)	$\pm\Delta\sigma_{stat}$ (mb)	$\pm\Delta\sigma_{total}$ (mb)
6.96	0.416	0.004	+0.016–0.019
7.93	0.675	0.006	+0.018–0.026
8.78	0.863	0.008	+0.025–0.039
9.85	0.974	0.006	+0.023–0.041
10.85	1.041	0.006	+0.026–0.045
11.78	1.020	0.005	+0.035–0.053
12.00	1.051	0.005	+0.032–0.040
12.78	1.033	0.005	+0.026–0.044
14.05	0.964	0.009	+0.037–0.043
14.95	0.912	0.010	+0.030–0.037
15.95	0.855	0.007	+0.041–0.047

[a] Centroid energy. The energy spread (FWHM) is about 2% below $E_\gamma = 10$ MeV and approaches 2.5% at 16 MeV.

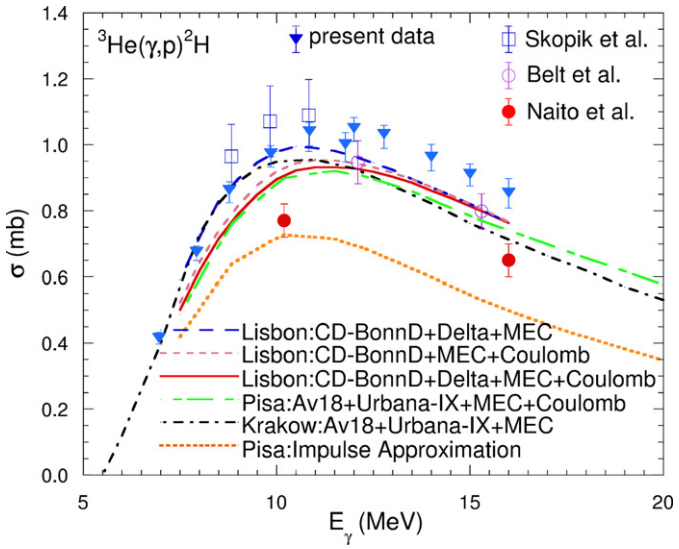

Fig. 5. (Color online.) Comparison of experimental data and theoretical calculations for the ^{3}He(γ, p)^{2}H total cross section. The present data are shown as inverted solid triangles. See text for explanation of the curves.

shown in Fig. 5 by inverted solid triangles were obtained. The error bars of 4 to 6% reflect the overall uncertainty (the individual uncertainties were added in quadrature) which is governed by the scale uncertainty associated with the absolute photon-flux determination of about +2% and −4%.

In order to compare to our data, and not clutter Fig. 5 too much, we selected representative data sets from the upper band (Skopik et al. and Belt et al.) and lower band (Naito et al.) of the data shown in Fig. 1. Clearly our data belong to the upper band. They are in fair agreement with the data of Skopik et al. and Belt et al. and also with the less accurate data of Kundu et al. and Fetisov et al. However, they are in clear disagreement with the recent data of Naito et al. and all the other data of the lower band. The present data provide systematically ∼10% larger cross-section values than predicted by theory in the entire energy range investigated. The long-dashed, short-dashed, and solid curves are calculations from the Lisbon group [21] extending up to 16 MeV. Here, the long-dashed curve is based on the potential CD-Bonn + Delta (CD-BonnD) [22], while 3NF effects are included via Delta excitations. In these calculations MECs are included, but the Coulomb interaction is neglected. The short-dashed curve gives the result with the Coulomb interaction included, but without Delta degrees of freedom. The solid curve represents the full calculation, *i.e.*, CD-BonnD + Delta & MECs and with the Coulomb interaction taken into account. The difference between the long-dashed and solid curves is a measure of the importance of Coulomb effects, while the difference between the short-dashed and solid curves shows the magnitude of 3NF effects. 3NF effects are surprisingly small for this observable. The long-dashed-short-dashed curve extending up to 20 MeV present the result of the Pisa group [23], which includes 3NF effects, and the Coulomb interaction. The Pisa group employs the Av18 NN potential and the Urbana IX 3NF. The MECs include two- and three-body contributions, which are constructed to exactly satisfy the continuity equation with the NN + 3NF model used. Note that the results obtained in the impulse approximation, without inclusion of MECs, underpredict most of the available experimental data above 10 MeV (see dotted curve). At energies below 12 MeV the Pisa group's full calculation is almost identical to the full calculation of the Lisbon group (solid curve). While the calculations of the Lisbon group are performed in momentum space using the screening and renormalization method of the Coulomb potential, the Pisa group's calculations are done in coordinate space with the unscreened Coulomb potential. The ^{3}He(γ, p)^{2}H reaction is dominated by electric dipole transitions (p-waves), which (in the long-wavelength limit) can be calculated by evaluating matrix elements of either the volume integral of the current density, $\int d\mathbf{x}\, \mathbf{j}(\mathbf{x})$, or the Siegert operator. The two forms are equivalent as long as the current is conserved [23]; of course, in the Siegert operator MECs are included implicitly. The first approach is used in the calculations of the Pisa group and the second in those of the Lisbon group – both these calculations take into account the Coulomb interaction. The corresponding results, which are quite close to each other, systematically underpredict the present data. Finally, the dashed-dotted curve which extends up to 20 MeV is the result of a calculation by the Kraków group [18] using the NN potential Av18 [19] plus the Urbana IX 3NF [20] with full treatment of meson-exchange currents (MECs). The Coulomb interaction is not included in this calculation.

The ∼10% discrepancy between the state-of-the-art theoretical calculations and our high-precision experimental data provides strong evidence that certain aspects of the three-nucleon dynamics are still not understood, as also documented by the few-nucleon analyzing-power puzzle [24] and the space-star anomaly [25]. At this point one can only speculate, but this is beyond the scope of the present work.

In conclusion, the present data for the ^{3}He(γ, p)^{2}H cross section clearly favor the upper band of data shown in Fig. 1. Therefore, we recommend to ignore the data of Wölfli et al., Naito et al., Ticcioni et al., and Matthews et al. for the comparison between experimental data and theoretical calculations.

Acknowledgements

The authors acknowledge valuable contributions received from M.W. Ahmed, A.S. Crowell, J.H. Esterline, S.S. Henshaw, C.R. Howell, E. Kwan, J. Li, S. Mikhailov, C. Sun, G.J. Weisel, and Y.K. Wu. This work was partially supported by the United States Department of Energy, Office of Nuclear Physics under Grants No. DE-FG02-97ER41033, No. DE-FG02-97ER41041, No. DE-FG02-97ER41042, and No. DE-AC05-06OR23177.

References

[1] S. Kölling, et al., Phys. Rev. C 80 (2009) 045502.
[2] S. Pastore, et al., Phys. Rev. C 80 (2009) 034004.
[3] T. Shima, et al., Phys. Rev. C 72 (2005) 044004.
[4] S. Naito, et al., Phys. Rev. C 73 (2006) 034003.
[5] W. Wölfli, et al., Phys. Lett. 22 (1966) 75.
[6] J.B. Warren, et al., Phys. Rev. 132 (1963) 1691.
[7] V.N. Fetisov, A.N. Gorbunov, A.T. Varfolomeev, Nucl. Phys. 71 (1965) 305.

[8] D.M. Skopik, et al., Phys. Rev. C 19 (1979) 601.
[9] J.L. Matthews, et al., Nucl. Phys. A 223 (1974) 221.
[10] A. van der Woude, et al., Phys. Rev. Lett. 15 (1971) 909.
[11] B.D. Belt, et al., Phys. Rev. Lett. 24 (1970) 1120.
[12] S.K. Kundu, Y.M. Shin, G.D. Wait, Nucl. Phys. A 171 (1971) 384.
[13] G. Ticcioni, et al., Phys. Lett. B 46 (1973) 369.
[14] G.M. Griffiths, et al., J. Canadian Phys. 40 (1962) 402.
[15] W. Tornow, C.A. Leckey, J.H. Esterline, G.J. Weisel, Nucl. Instrum. Methods Phys. Res. A 647 (2011) 86.
[16] R.E. Pywell, et al., Nucl. Instrum. Methods Phys. Res. A 606 (2009) 517.
[17] C. Sun, PhD dissertation, Characterization and diagnostics of Compton light source, Duke University, 2009.
[18] J. Golak, et al., Phys. Rep. 415 (2005) 89.
[19] R.B. Wiringa, V.G.J. Stoks, R. Schiavilla, Phys. Rev. C 51 (1995) 38.
[20] B.S. Pudliner, et al., Phys. Rev. C 56 (1997) 1720.
[21] A. Deltuva, A.C. Fonseca, P.U. Sauer, Phys. Rev. C 71 (2005) 054005.
[22] A. Deltuva, R. Machleidt, P.U. Sauer, Phys. Rev. C 68 (2003) 024005.
[23] L.E. Marcucci, et al., Phys. Rev. C 72 (2005) 014001.
[24] W. Tornow, Few-Body Syst. 43 (2008) 213.
[25] K. Sagara, Few-Body Syst. 48 (2010) 59.